

Identification and analysis of the young population in the starburst galaxy NGC 253

M. J. Rodríguez,^{1*} G. Baume^{1,2} and C. Feinstein^{1,2}

¹*Instituto de Astrofísica de La Plata (CONICET-UNLP), Paseo del bosque S/N, La Plata (B1900FWA), Argentina*

²*Facultad de Ciencias Astronómicas y Geofísicas - Universidad Nacional de La Plata, Paseo del bosque S/N, La Plata (B1900FWA), Argentina*

Accepted XXX. Received YYY; in original form ZZZ

ABSTRACT

We present a study of the young population in the starburst galaxy NGC 253. In particular, we focused our attention on searching young star groups, obtaining their main properties and studying their hierarchical organization. For this task, we used multi-band images and their corresponding photometric data obtained with the Advanced Camera for Surveys of the Hubble Space Telescope (ACS/HST).

We have first derived the absorption affecting the different regions of the galaxy. Then, we applied an automatic and objective searching method over the corrected data in order to detect young star groups. We complemented this result with the construction of the stellar density map for the blue young population. A statistical procedure to decontaminate the photometric diagrams from field stars was applied over the detected groups and we estimated their fundamental parameters.

As a result, we built a catalog of 875 new identified young groups with their main characteristics, including coordinates, sizes, estimated number of members, stellar densities, luminosity function (LF) slopes and galactocentric distances. We observed these groups delineate different structures of the galaxy, and they are the last step in the hierarchical way in which the young population is organized. From their size distribution, we found they have typical radius of $\sim 40 - 50$ pc. These values are consistent with those ones found in others nearby galaxies. We estimated a mean value of the LF slope of 0.21 and an average density of 0.0006 stars/pc³ for the identified young groups taking into account stars earlier than B6.

Key words: Stars: early-type – Stars: luminosity function, mass function – Galaxies: individual: NGC 253 – Galaxies: star clusters: general – Galaxies: structure – Galaxies: star formation

1 INTRODUCTION

Young star groups exist in a wide range of sizes, from compact star clusters to star complexes going through OB associations. Young open clusters contain a few tens to 10^5 stars in a typical diameter of a few parsecs and they are gravitationally bound (Morau 2016). OB associations are composed of young massive stars formed from the same molecular cloud, they are gravitationally unbound with low densities.

The distribution and properties of these systems are useful to understand the most recent history of the host galaxy as well as the star formation process under different environments. For this reason, in the last decades several works have been focused in performing global studies and

assembling catalogs of young stars groups over the nearest galaxies: LMC (Gouliermis et al. 2003), SMC (Battinelli 1991), M 31 (Bianchi et al. 2012), M 33 (Chandar et al. 1999; Bedin et al. 2005), NGC 6347 (Massi et al. 2015), NGC 300 (Pietrzyński et al. 2001; Rodríguez et al. 2016), NGC 7793 (Pietrzyński et al. 2005), M 81 (Nantais et al. 2010), M 101 (Bresolin et al. 1996), to name just a few.

In particular, the Sculptor Group galaxy NGC 253, is a barred almost edge-on spiral galaxy (SAB(s)c D, Vučetić et al. 2015), at a distance of 3.56 Mpc (Tully et al. 2013), which correspond to a projected linear scale of ~ 17 pc/arcsec. One of its most outstanding features is the starburst activity. Different works indicate that these bursts are located in the galactic central region up to ~ 300 pc in radius, with a star formation rate (SFR) of $\sim 2 - 3 M_{\odot} \text{ yr}^{-1}$ (Radovich et al. 2001; Ott et al. 2005), however their nature is not yet well understood. Accord-

* E-mail: jimenaro@fcaglp.unlp.edu.ar

ing to Engelbracht et al. (1998) the bursts are caused by the presence of the bar, that drives the gas into the central region. Additionally, Davidge (2010) suggested that the interaction with a now defunct companion occurred within the past ~ 0.2 Gyr, stimulating the formation of the bar and starburst activity.

Several young clusters were identified in the nuclear star forming region of the galaxy (e.g. Watson et al. 1996; Fernández-Ontiveros et al. 2009). One of them was associated with a super star cluster of $\sim 1.4 \times 10^7 M_{\odot}$ and an estimated age of 5.7 Myr. The simultaneous presence of red supergiants and OB stars in this cluster reveals several epochs of star formation (Kornei & McCrady 2009). Davidge (2016) found distinct substructures in it, suggesting that it is a star forming complex and not a single cluster.

The starburst activity added to its proximity make this galaxy an interesting candidate to study its young star population. In spite of this, there has not been made a detection of young star structures outside its central region. In this work, we carried out for first time the search and identification of young groups in NGC 253 adopting an automatic and objective searching method, and its subsequent analysis. We took advantage of excellent quality data from the Hubble Space Telescope (HST) that cover approximately the north-east side and the center of the galaxy (see Fig. 1).

The paper is organized as follows: In Sect. 2 we describe the observations and data sets, together with the reduction and data set-up. In Sect. 3 we presented the methods we used to search for and identify young stellar structures. Section 4 presents our analysis of the detected groups. We discuss our results in Sect. 5. Finally, in Sect. 6 we summarized our work and remark our main results.

2 DATA

2.1 Observations

The images used in this work were acquired from the Hubble Legacy Archive¹ and they were obtained in September 2006, as part of the program GO-10915 (PI: J. Dalcanton), during HST Cycle 15. These observations correspond to five fields of NGC 253, and were carried out with the Wide Field Camera (WFC) of the Advanced Camera for Surveys (ACS). The WFC has a mosaic of two CCD detectors with a field of view of $3'3 \times 3'3$ and a scale of $0''.049/\text{pixel}$. The five fields cover a total length of approximately $16'$ encompassing more than half of the galaxy (see Fig. 1). Three broad-band filters were used ($F475W$, $F606W$ and $F814W$), with total exposure times of 1482 s., 1508 s. and 1534 s. respectively, excepted the Field 1, which has higher exposure times: 2256 s. ($F475W$), 2283 s. ($F606W$) and 2253 s. ($F814W$).

2.2 Photometry

Binary FITS tables of photometry were obtained from the database of the Space Telescope Science Institute (STScI)². They correspond to the “star files” from the ACS Nearby

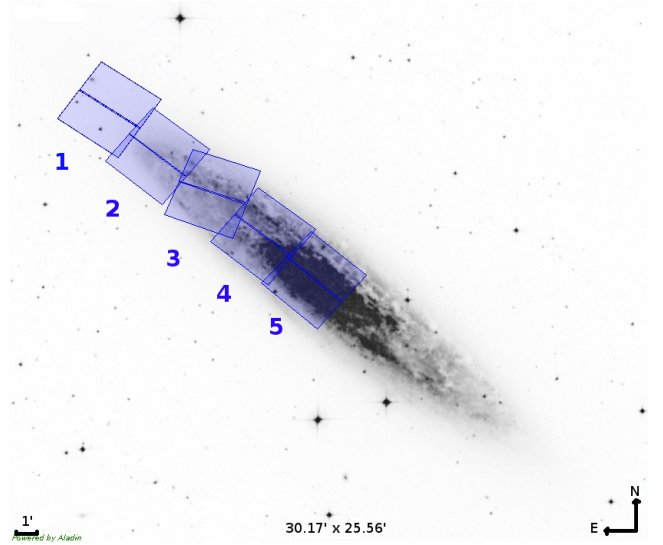


Figure 1. Distribution of the different HST/ACS fields (rectangles) used in this work overlaid on a Digitized Sky Survey (DSS) image of NGC 253. The North is up and East is left, the image cover $30'.1 \times 25'.5$.

Galaxy Survey (ANGST). These files contain the photometry of all objects classified as stars with good signal-to-noise values ($S/N > 4$) and data flag < 8 . These data were obtained performing point spread function (PSF) photometry using the package DOLPHOT adapted for the ACS camera. The reduction procedure was explained in detail in Dalcanton et al. (2008). In Fig. 2 we show the photometric errors in the different bands for the field 1 and 5, which are, respectively, the fields with the lowest and highest stellar density. To evaluate the completeness of the data, we built the luminosity function (LF) for the five studied fields (see Fig. 3). The number of stars per bin starts to decrease at $F606W \sim 26.5$. Therefore we considered that the sample is complete up to this value.

2.3 Photometric correlation of tables

Three photometric tables per field (in total 15 tables) were obtained from the ANGST, each one provide photometric information of only two bands. In order to join the three magnitudes in a single table for field, we used the code STILTS³ to perform a cross-correlation (with logical “OR”) between tables with $F606W - F475W$ bands and those with $F814W - F606W$ bands, obtaining five photometric tables, one for each field.

Furthermore, the adjacent fields slightly overlap each other (see Fig. 1), therefore we used STILTS to join the information of the five fields in one single table with approximately 3×10^6 objects. For this purposes, for the objects in the overlap region we took a final magnitude that results from the average between the stars in each field. Then we slightly shifted the coordinates of all the field to agree with those given at Gaia Data Release 1 (Gaia Collaboration et al. (2016); see Table 1).

¹ <http://hla.stsci.edu/>

² MAST: <https://archive.stsci.edu/>

³ <http://www.star.bris.ac.uk/~mbt/stilts/>

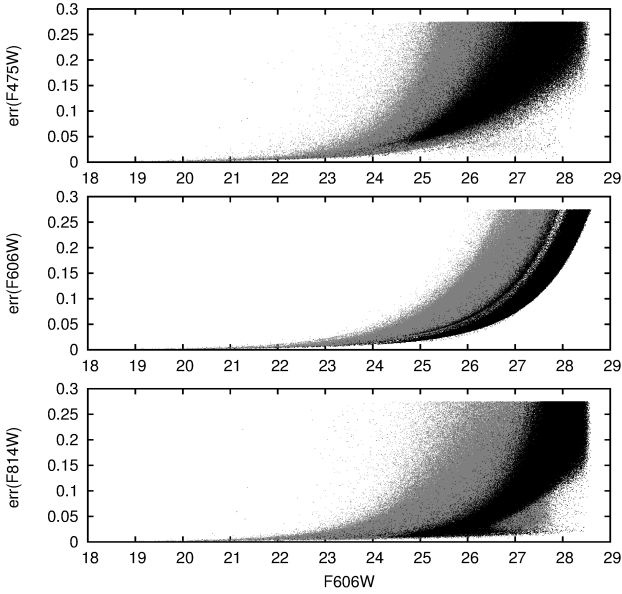


Figure 2. Photometric errors in the bands $F475W$ (top), $F606W$ (middle) and $F814W$ (bottom) vs. $F606W$ magnitude for the fields 1 (black) and 5 (grey).

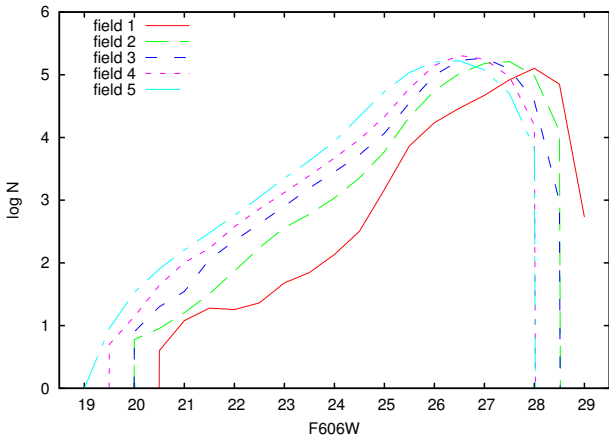


Figure 3. Observed LFs. There is a curve for each studied field.

3 IDENTIFICATION OF YOUNG GROUPS

As a previous step to identify star groups over the galaxy field, it was necessary to study a couple of problems present in our data sample. They were the following ones:

(i) Notwithstanding, the ACS/HST provide images with a high spatial resolution ($\sim 0''.05$), it is possible that, in the crowded regions of NGC 253, some objects identified as single sources are really blends of two or more ones, or even compact star clusters.

(ii) NGC 253 is heavily obscured at visible wavelengths, specially in its central region, due to its large amounts of dust (Pence 1980). This causes that the detected objects appear redder than its real color, making it difficult to identify young blue star populations.

Table 1. Astrometric (top table) and photometric (bottom table) corrections applied to obtain the final catalog (see text for details).

Field	$\Delta\alpha \cos(\delta) ["]$	$\Delta\delta ["]$
5-gaia	-0.056	0.078
4-5	0.278	-0.480
3-4	0.252	0.285
2-3	-0.022	0.022
1-2	-1.055	-0.096

The first column is: (field shifted)-(field to coincide).

Field	$\Delta F475W$	$\Delta F606W$	$\Delta F814W$	N
4-5	0.011 ± 0.082	0.036 ± 0.073	0.047 ± 0.081	221
3-4	0.119 ± 0.183	0.081 ± 0.115	0.047 ± 0.099	45
2-3	-0.076 ± 0.119	-0.015 ± 0.082	-0.003 ± 0.067	162
1-2	-0.001 ± 0.015	-0.042 ± 0.017	0.047 ± 0.017	2

N is the number of stars in the two fields.

3.1 The blending problem

Several previous works have studied this problem (e.g. Renzini 1998; Kiss & Bedding 2005). In our case, to obtain a measure of the importance of the blending effect, we followed the reasoning presented by Kiss & Bedding (2005). Therefore, we performed several numerical simulations using random distributed stars with a uniform spatial distribution, a power law distribution in bright, ranging from 18 to 27, and a uniform distribution in color, ranging from 0 to 2. We analyzed different stellar densities cases ranging from 1 star/arcsec² to 10 stars/arcsec². This range of values correspond to those found along the galaxy, but remarking that the highest ones only were present in a few special places of the galaxy (see in advance Fig. 8). Therefore, for a given stellar density value, we build the corresponding bidimensional spatial histograms with a binning step of $0''.07$ to obtain binned areas that simulate the ACS/HST resolving power. We could then evaluate the total amount of objects with blending in each simulation. To evaluate the error in magnitudes and colors due to this effect, we computed the total magnitude and color on each bin and we compared these values with the corresponding ones to the brightest star in that bin. The above procedure was repeated five hundred times for each stellar density. As a result, we obtained that the error in magnitude, as expected, have an increasing behavior with the stellar density value. Therefore, in the worst case (10 stars/arcsec²), we found that the percentage of stars that had an error in magnitude greater than 0.1 mag increased from almost null values for bright stars ($F606W \sim 18$) to only 2% for stars of magnitude $F606W = 24$. Regarding the behavior in color, we found, again for 10 stars/arcsec², that at most 15% of the stars have errors in colors larger than 0.1 mag and this value was approximately independent of the magnitude value. These obtained figures for both errors in magnitude and colors revealed that notwithstanding the blending effect was still present using ACS/HST data, the amount of stars that reached errors of 0.1 mag were only a small fraction of all the objects, at least for the studied stellar densities.

3.2 The absorption problem

To estimate the visual absorption (A_V) along the galaxy, we selected the brightest objects ($F606W < 24$) and compared their locations on the color-magnitude diagrams (CMDs) with the theoretical evolutionary model PARSEC version 1.2S (Tang et al. 2014) with $Z=0.0152$ corresponding to 10^7 yr. Assuming as a first approximation that all the selected brightest objects belong to the main sequence, it was possible to deredden their location on the CMDs and estimate approximately their individual absorption values. This procedure could include intrinsically red stars that would produce overestimated A_V values. Therefore, we minimized this effect, and a possible blending effect, assigning to each star the minimum A_V value in a surrounding spatial region with at least 10 stars. We adopted a single isochrone to obtain the absorption values for a sample of stars that could cover a wide range of ages and/or metallicities.

The results of the indicated procedure could be sensitive to the crowding/blending present in the galaxy and/or to the adopted isochrone model. To check the former issue we computed the absorption maps for three $F606W$ magnitude ranges (8.8 - 23.2; 23.2 - 23.7 and 23.7 - 24.0) in such way that we have the same amount of stars (11222) for each group. The obtained absorption maps did not show significant differences among themselves or with the map obtained considering the entire range of bright stars ($F606W < 24$). The comparison of the different maps allowed us to estimate an error in our results $e_{A_V} \sim 0.09$ mag. On the other hand, our numerical simulations (see Sect. 3.1) and the use of different isochrones revealed that the employed procedure to estimate the absorption values along the galaxy provides enough precision for a first search of young star groups.

In the left panel of Fig. 4 we present the obtained absorption map of the observed region of NGC 253 following the above procedure. In this figure we did not include the most external field (Field 1, see Fig 1), because it presented several foreground stars or background galaxies and very few bright stars belonging to the galaxy, so it introduce many spurious detections. The obtained absorption map was used then to correct the observed magnitudes of the brightest objects. This is: $(F475W)_0 = F475W - A_{F475W}$; $(F606W)_0 = F606W - A_{F606W}$ and $(F814W)_0 = F814W - A_{F814W}$. For this task, we use the corresponding absorption value for each filter, that were estimated using the coefficients $A_{F475W}/A_V = 1.192$, $A_{F606W}/A_V = 0.923$ and $A_{F814W}/A_V = 0.605^4$ (O'Donnell 1994). In the right panel of Fig. 4 we show a WISE IR false color image of the same NGC 253 region shown in the left panel. It was obtained from the combination of the W3 and W4 bands, which best map the dust content. We could note that the regions with stronger absorption correspond to the brightest areas (highest dust content), they are the nucleus, the bar, and the most inner spiral arms.

3.3 Selecting blue and red objects

To split the selected brightest objects between intrinsic blue ones and those probably identified with red stars, we used

the following criteria: a) $F475W_0 - F606W_0 < 0.5$ and $F606W_0 - F814W_0 < 0.5$ for adopted *blue objects*, and b) $F475W - F606W > 1$ and $F606W - F814W > 1$ for adopted *red objects*. For this last group we considered only those objects that were not include in the blue sample. It is important to note that the first group were selected over the corrected magnitudes, the red objects instead were selected using the observed magnitudes. We used then the *blue objects* to detect young star groups. A combination of Hess diagrams and CMDs diagrams of all the detected objects are showed in the top panel of Fig. 5. In the bottom panel we showed the the CMDs of each selected group where the diffuse border between *blue* and *red objects* reveals the strong dispersion of the absorption values present along the galaxy.

3.4 Searching method

With the aim of identify young star groups in NGC 253, we employed the Path Linkage Criterion (PLC Battinelli 1991) over the *blue objects* selected above. The main idea of the technique is that two objects belong to the same star group if it is possible to connect them by successive links of *blue objects*. The link distance between selected objects has not to be larger than a fixed parameter called search radius d_s . A young star group is detected when it is possible to link more than p objects. To adopt adequate values for the parameters d_s and p , we plot in Fig. 6 the number of identified groups using the PLC as a function of d_s for different p values. A good choice for the parameter d_s is set by the maximum number of groups detected for a given p value (Pietrzyński et al. 2001). Figure 6 reveals this maximum is located for d_s between 1.5-2 arcsec. Based on these values, and with the caution of detect the smallest subgroups of each large association or stellar complex, we adopted a more extended range of d_s , covering the range 0.3-2 arcsec (~ 5 -34 pc at 3.56 Mpc; Tully et al. 2013). Using this criteria, the method identified first the smallest groups using $d_s = 0.3$ arcsec, then this value was increased using a step of 0.4 arcsec and the PLC method was run again over the remaining *blue objects*. This procedure was repeated until d_s reached 2 arcsec value. Regarding the parameter p , it must be chosen prudently. While a low value results in many spurious detections, a high one may cause the lost of the smallest groups. We studied then the obtained results with different p values (see Fig. 6). We also noticed that in a similar study for NGC 300 galaxy, Rodríguez et al. (2016) adopted $p = 10$ stars, however for NGC 253 we are leading with a more distant galaxy and there is probably a blending effect of the individual objects in the used ACS images. Therefore, we considered $p = 8$ objects as a reasonable value.

Employing the described procedure, we detected 897 individual groups of young objects. However, a few of these groups were spurious detection caused bright foreground stars, which caused noise spikes in the extended PSFs, or background galaxies, which were identified as faint extended diffuse objects. These false detections were located mostly in Field 1 and in Field 5. Removing these spurious detections manually, we obtained a final list of 875 young star groups. These groups are show in Fig. 7 over an infrared

⁴ <http://stev.oapd.inaf.it/cgi-bin/cmd>

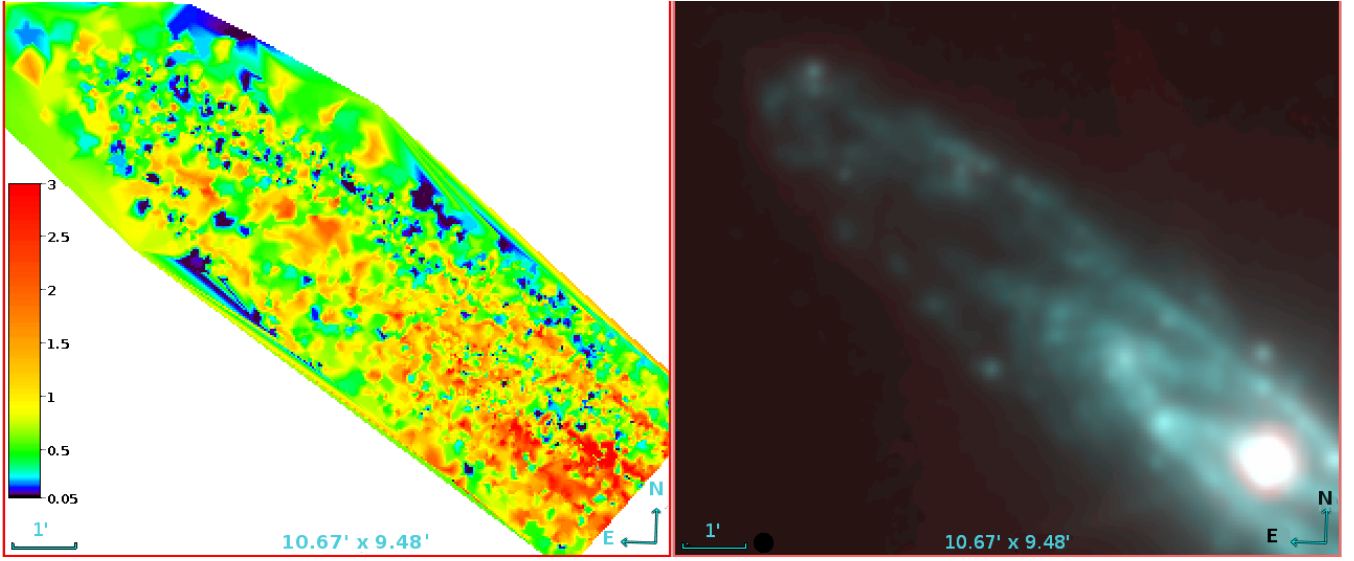


Figure 4. *Left:* Visual absorption (A_V) map of the observed region of NGC 253. *Right:* WISE IR color image of NGC 253, obtained by the combination of the W3 and W4 bands. A color version of this figure and a FITS version of the absorption map are available online.

WISE⁵ false color image of the galaxy. It can be noted the good agreement between their distribution and large galactic structures as the galactic spiral arms and the central bar (see Sects. 3.6 and 5.3).

3.5 Stochastic detections

To evaluate the fraction of star groups found using the PLC that could be stochastic gatherings of stars and not real groups, we ran numerical simulations using randomly distributed sources with similar star densities to three selected regions, which have very different stellar density values. These are: 1) the region at ~ 2 arcmin NE of the galactic nucleus, 2) a place in one of the spiral arms and 3) a region between the spiral arms. In each region we measured the mean stellar density of the *blue objects*, and we respectively found the following values: 1) $\rho = 0.635$ stars/arcsec², 2) $\rho = 0.203$ stars/arcsec² and 3) $\rho = 0.028$ stars/arcsec².

The first region is the densest, close to 0.64 *blue objects* per arcsec. This high density means that the average distance among stars is $0''.70$. So, running PLC algorithm to similar search radius or greater the method will find all the star belonging to one single cluster that is a collection of all the stars. Using $0''.3$, the lowest search radius that we have used for the real data, we found one stochastic cluster in four cases from 10000 experiments, a very low number. Increasing the d_s value, the obtained numbers were still low, for example for $d_s = 0''.4$ we found 149 clusters in 10000 experiments. We noticed that the stellar groups found by PLC over the numerical simulations had ‘; “worm” shapes. This means that they seemed as extended twisted line, and they did not have any circular shape as would be expected for real star groups. Therefore, most of the stochastic clusters did not pass a simple visual inspection. We did not found

any stochastic cluster for the cases 2) and 3) for $d_s = 0''.3$ and a very few for higher search radius.

3.6 Identifying large young structures

Larger young stellar structures could be found using the PLC with even larger searching radius or building the stellar density map. We choose this last option since it produces better and clear results.

To build the corresponding density map we constructed a two dimensional histogram counting the numbers of objects in spatial bin sizes 8×8 arcsec². Then, we applied the drizzle method considering a 2.0 arcsec step (see Fruchter & Hook 2002, for details of this method). Over this map we plotted isodensity at several values: 40, 80, 110, and 145 stars per bin of 8×8 arcsec².

The stellar density map with the different contours is presented in Fig. 8. Here we also can identify how the blue population delineates the spiral arms of the galaxy. Furthermore, the way in which larger structures enclose smaller and denser ones point out a hierarchical behavior of the young population. We would discuss this result in Sect. reffierarchical.

4 ANALYSIS

We performed an automatic analysis of the detected young star groups using a numerical code developed in FORTRAN 95. This code allowed the study of selected groups in a systematic and homogeneous way. The code estimated the basic parameters of each group detected by the PLC, as their sizes, densities, amount of objects members, and build their CMDs and LFs, with their corresponding slope values.

Table 2 presents the first ten rows of the resulting catalog, in which are listed the properties for each of the 875 young groups. The complete version is only available online.

⁵ <http://wise.ssl.berkeley.edu/>

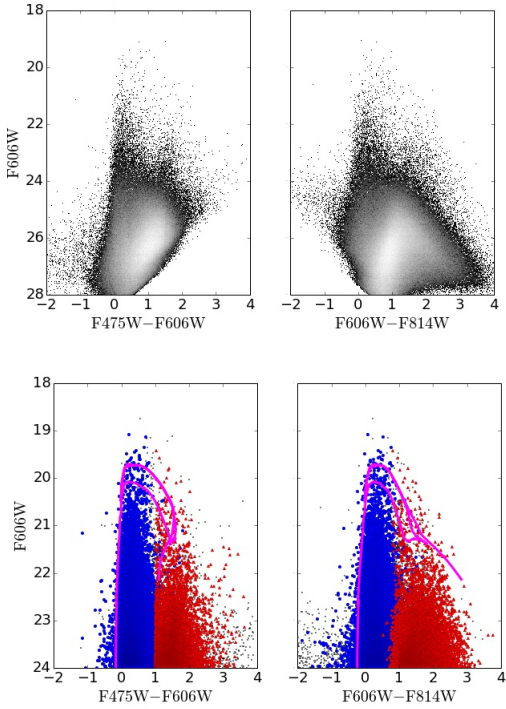


Figure 5. *Top panel:* Combined Hess diagrams and CMDs with all the detected objects over the total covered region in NGC 253. The different grey shades indicate the stars relative density from black (less dense) to white (more dense). *Bottom panel:* Blue circles and red triangles indicate the selected brightest blue and red objects (see Sect. 3.3). The pink line indicates the PARSEC version 1.2S isochrone Tang et al. (2014) corresponding to 10^7 yr and metallicity $Z=0.0152$, displaced adopting a distance modulus of $(V_o - M_V) = 27.75$ (Tully et al. 2013), a normal reddening law ($R = A_V/E(B - V) = 3.1$) and a value for $E(B - V) = 0.016$ corresponding to the foreground reddening toward NGC 253 (Schlafly & Finkbeiner 2011). A color version of this figure is available online.

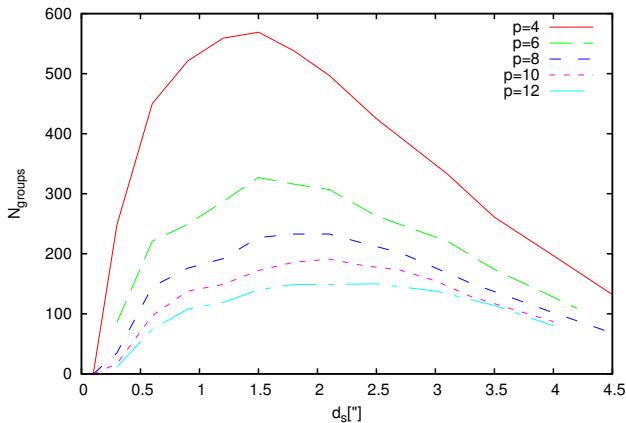


Figure 6. Behavior of the number of groups detected using the PLC technique as a function of the parameter d_s for different values of the parameter p .

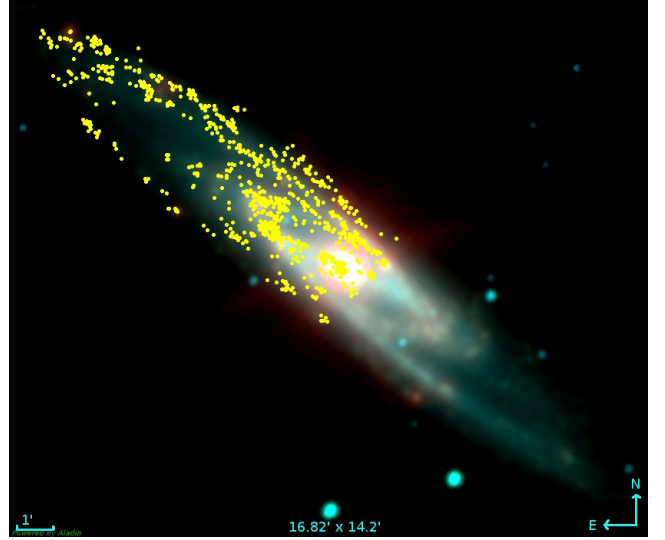


Figure 7. Detected young groups (yellow symbols) over an infrared WISE false color image of NGC 253. The image covers $16.82' \times 14.2'$ the North is up and East is left. A color version of this figure is available online.

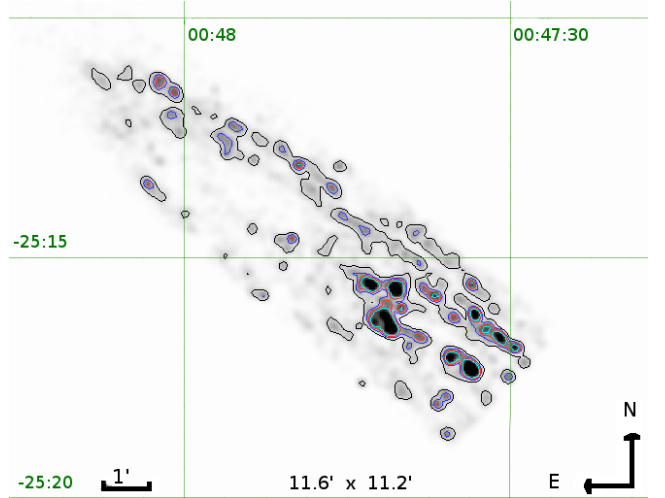


Figure 8. Stellar density map of blue stars, the overlapping contours correspond to different density levels: 40, 80, 110, 145 stars per bin of 8×8 arcsec². The image field is $11.6' \times 11.2'$, the North is up and East is left. A color and a FITS versions of this figure are available online.

4.1 Sizes and densities

The location and size of each group (α_{J2000} , δ_{J2000} and radius, r) were computed, respectively, as the mean and two times the radial standard deviation (σ) of the location of the corresponding objects identified by the PLC method. An approximate value of the groups stellar density could be estimated counting the total numbers of stars in a volume of πr^3 (see Table 2).

4.2 Field star decontamination

To better study each group, our code decontaminated their corresponding CMDs from field stars performing a statistical cleaning. The clean method was based in the comparison between the CMD for a young group region and the CMD for a corresponding field region located near that group and covering the same sky area. Therefore, those objects with similar positions over both CMDs were eliminated in the CMD of the group region (see Gallart et al. 2003, for details).

The above procedure was applied taking into account the color indexes $CI1 = F475W - F606W$ and $CI2 = F606W - F814W$ simultaneously. For each star in the region we calculated the distance in the CMDs with all the star in the field. The most similar star in the field provided the minimum distance value, if this value was less than a given tolerance, then the star in the group region was subtracted. The CMD distance was calculated using the following expression:

$$\{(F606W_r - F606W_f)A\}^2 + \{(CI1_r - CI1_f)B\}^2 + \{(CI2_r - CI2_f)B\}^2$$

where the subscripts “*r*” and “*f*” refers to stars in the region and field respectively and the constants *A* and *B* are normalization factors.

In order to obtain a field region as homogeneous as possible, avoiding possible neighbor groups or to fall outside the field of view. The code choose five different field regions for each group. The first region is a ring around the studied group, and the others are selected as follows: $(\alpha_0 \pm \Delta\alpha, \delta_0)$; $(\alpha_0, \delta_0 \pm \Delta\delta)$ where $\Delta\alpha = \Delta\delta = 11''.6 \sim 200$ pc. Then the fields with the maximum and minimum number of stars were discarded, and the final decontamination result is an average of the decontamination obtained with the three remaining field regions.

4.3 Color-magnitude diagrams

We built the decontaminated CMDs, $F606W$ vs. $F475W - F606W$ and $F606W$ vs. $F606W - F814W$ for each star group, taking into account the blue and red population identified in Sect. 3.3.

In Fig. 9 we show the CMDs of three young groups. We overlapped the evolutionary models of PARSEC version 1.2S corresponding to 10^7 yr (gray line) and 10^9 yr (pink line) with solar metallicity for comparison. These models were displacing adopting a distance modulus of $(V_0 - M_V) = 27.75$ (Tully et al. 2013), a normal reddening law ($R = A_V/E(B - V) = 3.1$) and a value for $E(B - V) = 0.016$ corresponding to the foreground reddening toward NGC 253 (Schlafly & Finkbeiner 2011). In these diagrams we can note that a small group of *red objects* still prevails. This is because in the right region of the diagrams the stars are more dispersed, causing that the statistical subtraction lose efficiency. Nevertheless, we could see that for the *blue objects* the statistical subtraction is more reliable.

4.4 Luminosity function

The $F606W$ LF of the brightest end of each detected young group were build using only the selected *blue objects* inside the corresponding radius *r* (see Sect. 3.3) and adopting a bin interval of 0.5 mag. The LF slopes, $\Gamma = d \log N / d F606W$,

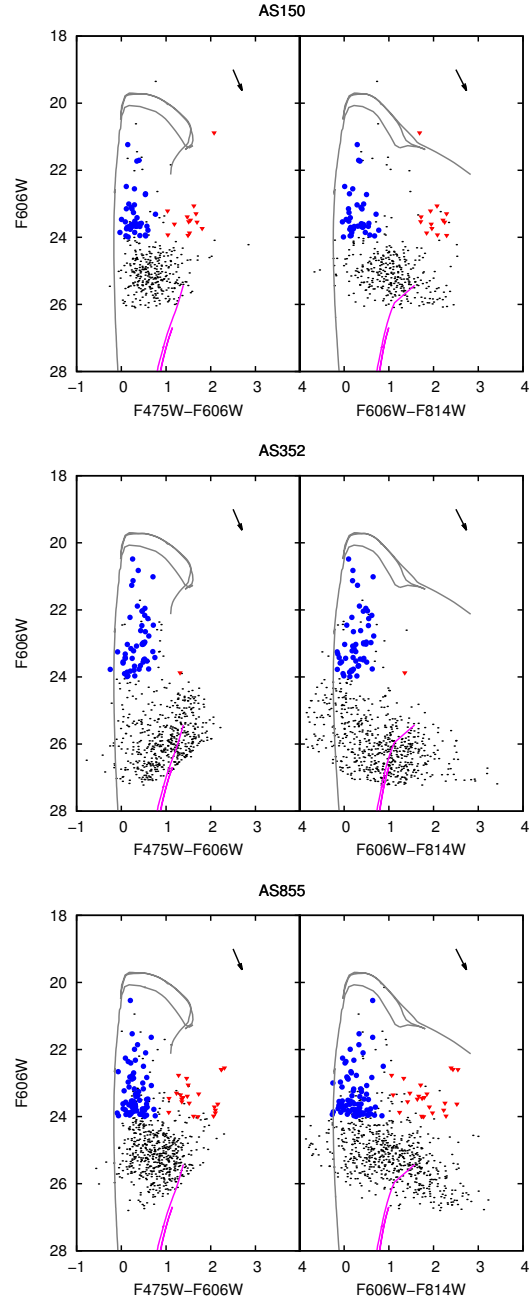


Figure 9. Decontaminated CMDs $F606W$ vs. $F475W - F606W$ and $F606W$ vs. $F606W - F814W$ of the star groups AS150, AS352, and AS855, that are located in different galactocentric distances. The meaning of symbols is explained in the text (Sect. 4.3). The grey and pink lines indicates the isochrones corresponding to 10^7 yr and 10^9 yr respectively and metallicity ($Z = 0.0152$). (Tang et al. 2014). The arrow indicates the reddening vector. A color version of this figure is available online.

were determined performing a linear least squared fit. The obtained slopes are listed in Table 2.

In Fig. 10 we present the LFs for the groups AS 150, AS 352 and AS 855, the straight lines indicate the linear fits and the indicated errors correspond to $N^{1/2}$, where *N* is the number of stars in each 0.5 magnitude bin.

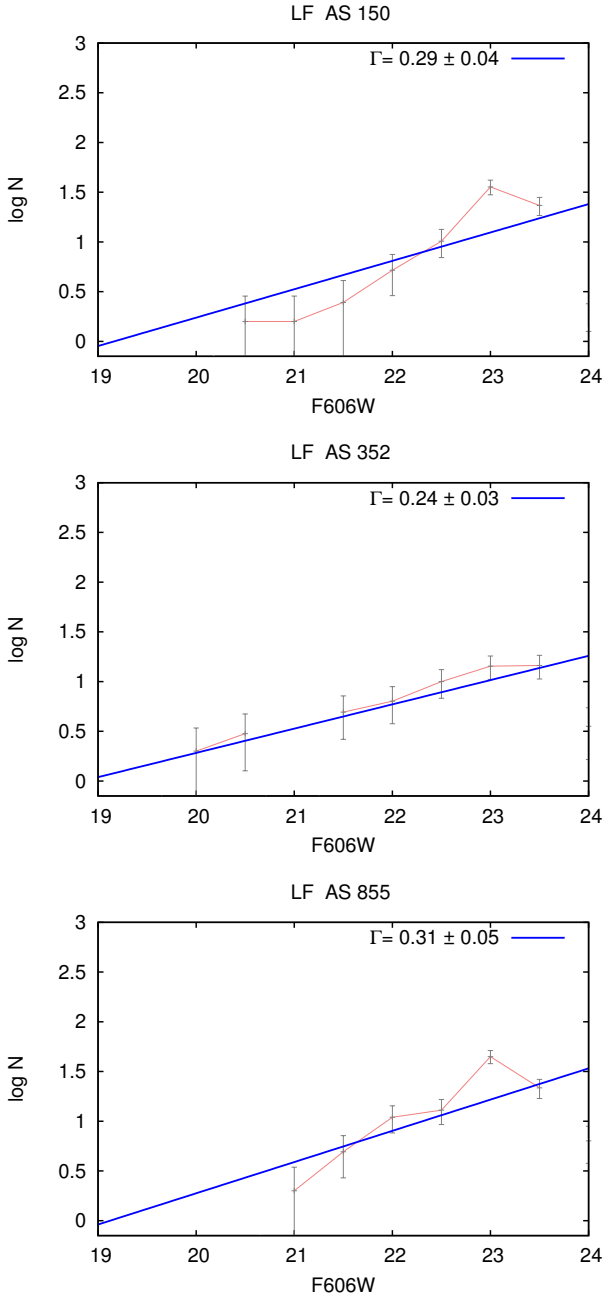


Figure 10. LF of three young star groups located at different place in the galaxy, AS 150, AS 352 and AS 855. The line indicates a linear fit over the considered bins (see Sect. 4.4), the slope estimated in each case is indicated in the top right corner.

The mean slope was derived considering only the groups with more than 30 bright members and $\text{err}_\Gamma \leq 0.05$, obtaining a value of 0.21.

5 DISCUSSION

5.1 Comparison with NGC 300

We compared our detected young groups with those identified in NGC 300, which were studied by Rodríguez et al.

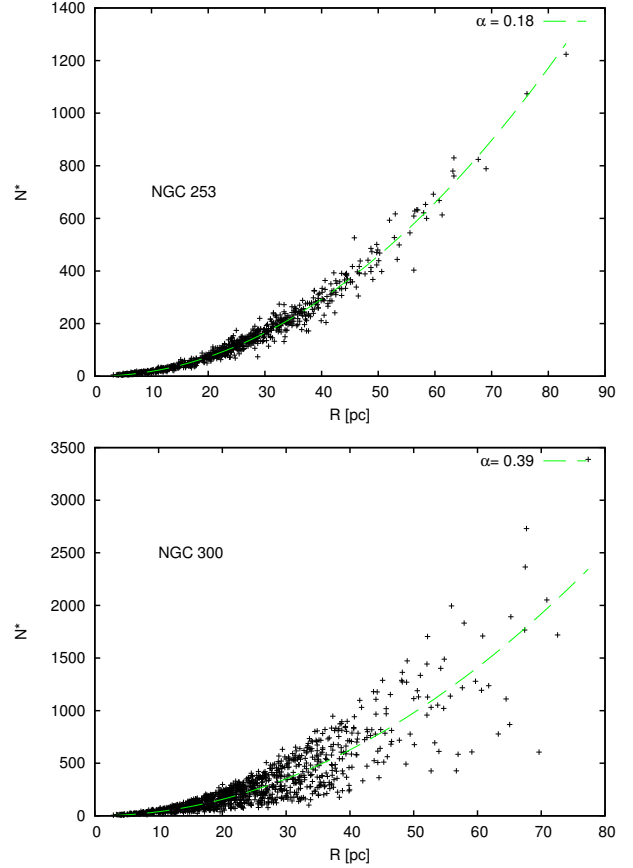


Figure 11. Number of stars members vs. radius of young groups, for NGC 253 (top) and NGC 300 (bottom). The dashed line correspond to a quadratic fit over the data.

(2016) using similar observational data that in the present work.

In Fig. 11 we plotted the number of stars members versus the size of the groups in each galaxy. To be consistent with Rodríguez et al. (2016) we adopted in this figure a radius of 1σ (the radial standard deviation of the groups member location). We performed a quadratic fit to the data, in order to compare the numbers of members detected in groups of the same size in both galaxies. The least squared fit was performed taking into account the groups with sizes larger than 9 pc, to avoid the most crowded regions. We found a ratio of ~ 2 between the quadratic coefficients (α) of each galaxy. In other words, the associations in NGC 300 would appear to contain twice as many stars as NGC 253.

However, NGC 300 is located almost half the distance to NGC 253, therefore in this galaxy we were reaching less luminous objects than in NGC 253, or less massive main sequence stars. Thus, it was expected that we could detect more members in the NGC 300 associations, but this was only a distance effect.

5.2 Hierarchical structure in NGC 253

As was mentioned in Sect. 1, star forming regions exist in a wide range of sizes, from the compact star cluster to the spiral arms of a galaxy. Using the PLC and the stellar density map (Sects. 3.4 and 3.6), we have searched and identi-

Table 2. Catalog of young star groups in NGC 253

name	raj2000 (deg)	dej2000 (deg)	r [pc]	N	N_{dct}	$N_{dct-bri}$	$F606W_{bb}$	dens[* / pc ³]	LF slope (Γ)	err Γ	d_{GC} [Kpc]	A_v
AS002	11.911189	-25.250842	14.80	48	32	18	19.99	0.00314	0.12	0.03	3.91	0.610
AS003	11.894225	-25.283620	13.77	31	23	19	19.85	0.00280	0.04	0.05	0.47	0.610
AS004	11.872012	-25.281292	15.15	31	20	17	18.45	0.00183	0.03	0.04	3.07	0.610
AS006	11.881036	-25.286077	18.59	54	34	12	20.77	0.00169	0.02	0.05	1.26	0.050
AS007	11.909739	-25.280824	11.36	26	15	9	20.94	0.00326	0.02	0.05	1.85	0.050
AS008	11.920171	-25.274954	8.26	22	16	9	23.12	0.00903	0.03	0.02	2.58	0.050
AS009	11.888770	-25.289815	17.90	46	29	22	20.26	0.00161	0.02	0.05	0.24	0.050
AS010	11.958507	-25.243423	23.41	105	71	44	19.18	0.00176	0.21	0.03	5.05	0.190
AS011	11.877059	-25.280397	10.33	24	18	11	21.80	0.00520	0.07	0.04	2.58	0.190
AS012	11.910848	-25.277194	12.74	35	27	18	19.77	0.00416	0.10	0.05	1.72	0.190

The suffix *bri* indicates bright stars with $F606W < 24$.

The suffix *dct* indicate stars belonging to the decontaminated region.

$F606W_{bb}$ is the $F606W$ value of the brightest blue object in the group.

d_{GC} is the galactocentric distance.

A_v is the characteristic absorption affecting the group.

Here we present the first ten rows, the complete table is only available in electronic form.

fied an important number of young star groups whose sizes and amount of members revealed they include different kind of structures, from simple open clusters to important complexes of several OB associations. In Fig. 8 we could see how the largest and most scattered young structures enclose the densest and compact ones, going through different density levels, indicated by the different contours. In fact, if we plot the PLC groups together with the contours obtained from the density map, we see a large number of these groups within the densest contours (see Fig. 12), suggesting that they enclose stellar complexes.

This behavior of the young population is known as hierarchical structure (e.g. Elmegreen et al. 2000). We can see the relationships among these structures in Fig. 13, in which we presented the corresponding tree diagram or dendrogram. In the bottom, the diagram starts with the structures detected in the lower density level (40 stars per bin of 8×8 arcsec², black contour in Fig. 8). Most of these structures divide themselves in denser and smaller systems that are detected in the second density level (80 stars per bin of 8×8 arcsec², blue contour in Fig. 8). This behavior is repeated it turns through the more dense levels (110 and 145 stars per bin of 8×8 arcsec², red and turquoise contour respectively). Finally, we add a fifth level which correspond to the groups detected with the PLC method and contained in the structures detected in level 4. It is not possible to detect such groups in the density map because the map pixels sizes is 2 arcsec which is comparable to the groups size.

5.3 Distribution of the young star groups in the galaxy

As was indicated in Sect. 3.4, in Fig. 7 we show the distribution of the identified groups on an infrared WISE image of the galaxy. Therefore, it is possible to note that the stellar groups are mainly located over some special features of NGC 253, they are I) the nuclear region, II) the observed extreme of the bar, III) a ring like structure enclosing the bar, and IV) the spiral arms. All these structures are promi-

nent in the near infrared spectral range (see Fig. 4 of Iodice et al. 2014).

In particular, we found two stellar complexes with almost twenty members (individual young groups) near the central region of the galaxy (contours A and B in Fig. 12). The closer to the center (complex A) is within the 300 pc of starburst activity, and it is coincident with the super star cluster described in several works (eg. Kornei & McCrady 2009; Davidge 2016). Through the PLC method we could identify several individual star groups in this region, suggesting that it is in fact a stellar complex rather than a super cluster. The same conclusion was arrived by Davidge (2016) who found star formation in different locations inside this region.

We also can see in Fig. 7 a large stellar complex containing several groups at the edge of the bar, this complex is indicated with the contour C in Fig. 12, in this last optical image the bar is totally obscured by the dust and only are visible the star forming region in the bar edge. This knot and the other extreme of the bar were identified by Iodice et al. (2014) as bright points, in near infrared images of VISTA⁶, that connect the bar with the outer spiral arms. Their analysis suggest these knots as regions of local star formation instead of being the typically ansae observed in other barred galaxies, which is consistent with ours detections.

On the other hand, there was expected to find young groups in the ring structure, since this region is associated with active star formation as was suggested by the H_α maps of the region (Hoopes et al. 1996). The origin of this structure, with a radius between 2.6 and 3.1 kpc, is not yet well understood. According to Iodice et al. (2014) it is probably the result of a merge with a small satellite or, alternatively, it is an intermediate phase in the bar formation.

5.4 General properties of the young star groups

In Fig. 14 we show the size distribution of the star groups, we can see that the radius ranges from 5 to 150 pc with a

⁶ <http://www.vista.ac.uk/>

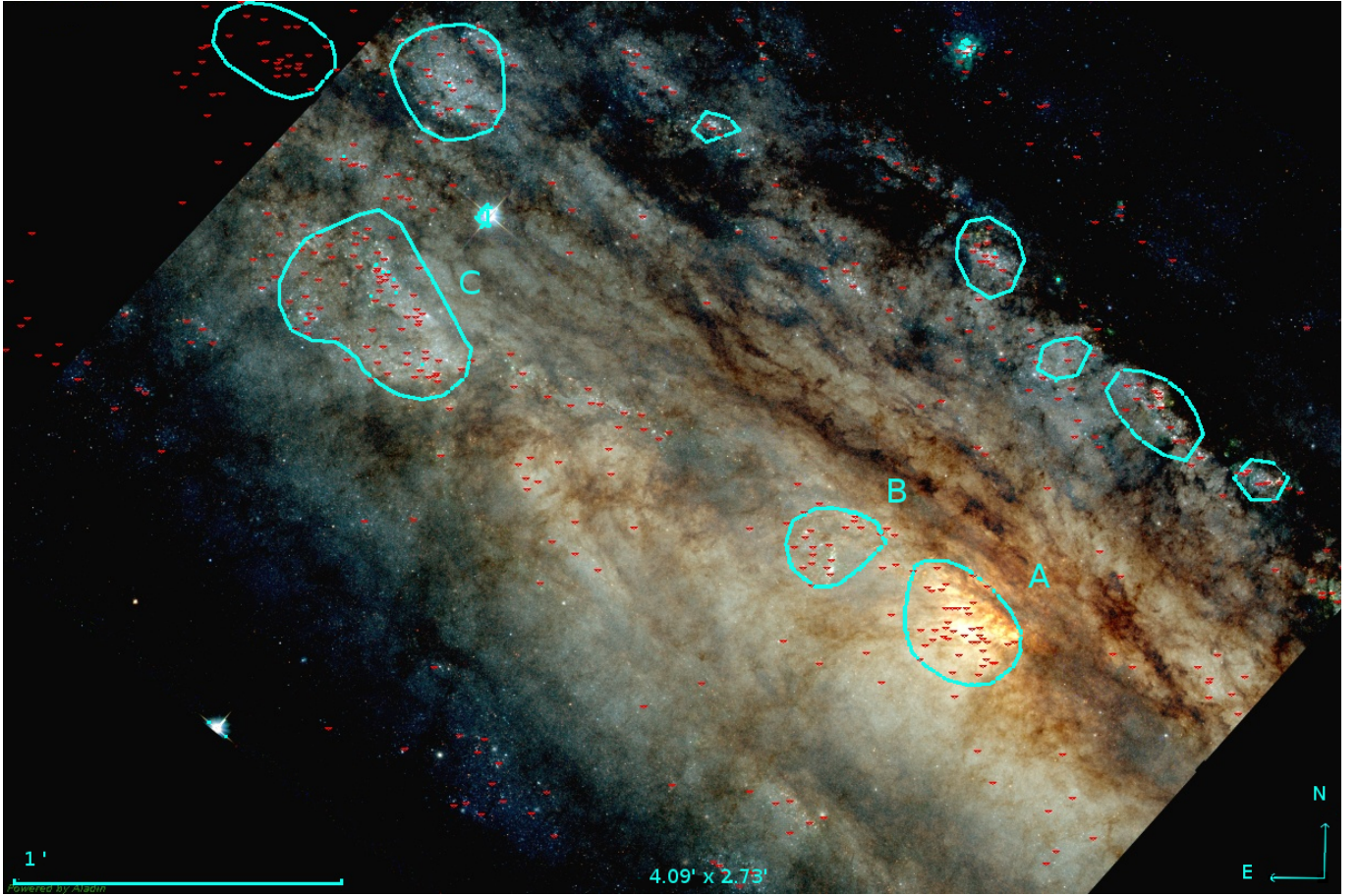


Figure 12. ACS/WFC color image of the field 5, obtained from the combination of the filter F475W in blue, F606W in green and F814W in red using ALADIN. The inverted triangles indicate the center of the individual groups detected by the PLC method, the contours are the densest that appear in Figure 8 Fig. 8 and indicate stellar complexes (see Sect. 5.2 and 5.3). A color version of this figure is available online.

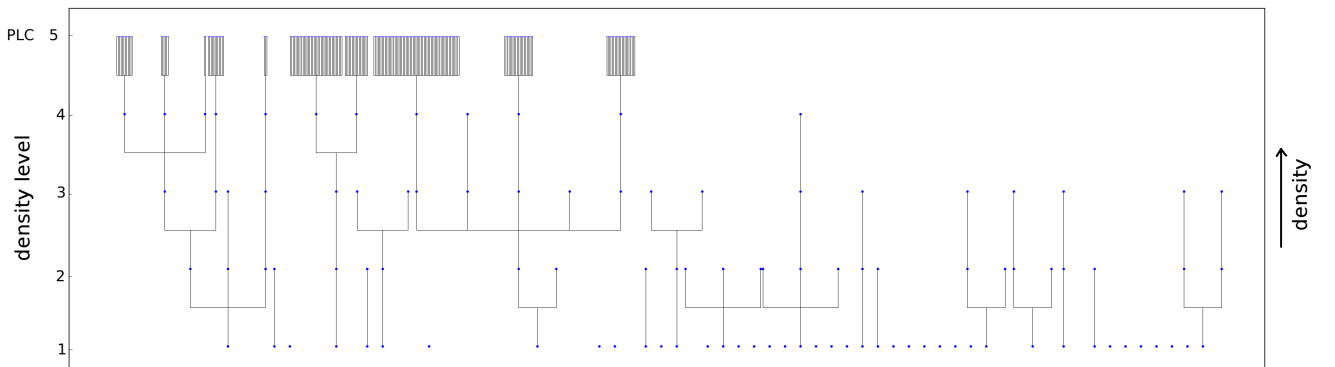


Figure 13. Dendrogram of the young stellar structures detected at different density levels. Levels 1 - 4 correspond to 40, 80, 110, and 145 stars per bin of $8 \times 8 \text{ arcsec}^2$, respectively. Level 5 corresponds to the most compact groups detected using PLC. The small circles indicate different stellar structures. Structures which are related in a hierarchical way are connected by solid lines.

peak close to 40 pc. We found an average radius of ~ 47 pc. These values are in good agreement with the OB association size found in others galaxies, using automatic search methods and HST images. Rodríguez et al. (2016) found a value of 25 pc for the mode and the average radius of young stars groups in NGC 300, although these values are lower than ours, we must consider that they used values of radius equal to 1σ instead of 2σ as in this work. Bresolin et al. (1998) studied the OB associations in seven spiral galaxies, NGC 925, NGC 2090, NGC 2541, NGC 3351, NGC 3621, NGC 4548, and M101, finding size distribution peaks between 25-45 pc and average radius a between 25-60 pc. In our Galaxy these values are somewhat smaller. Mel'Nik & Efremov (1995) found a maximum in the size distribution of 15 pc and an average radius of 20 pc in the OB associations with distances within 3 kpc of the Sun. For example, the associations in the Orion region Ori OB1a and Ori OB1b have radius of 37 pc and 17 pc respectively (Briceno 2008), the associations in Cygnus region have an extended range of radius from 10 to 70 pc Garmany & Stencel (1992).

In Fig. 15 we presents the trend of several parameters against the galactocentric distance. In the upper panel we show the $F606W$ magnitude value of the brightest star in the stellar groups for each 0.5 kpc bin; the middle panel presents the behavior of the red ($F814W$) background level measured on the ACS/WFC drizzle images; and the bottom panel indicates the stellar density values of bright stars. Both, the background levels and the stellar density values correspond to the same stellar groups indicated in the upper panel.

These figures allowed us to notice that the brightest stars in the stellar groups was decreasing up to distances ~ 6 kpc and then remained approximately constant. The behavior at the central part of the galaxy could be due to a blending/crowding effect, a change in the stellar density since it directly affect the chance to get a bright star for a given initial mass distribution, or a flatter slope of the mass distribution itself. The middle panel of Fig. 15 was adopted as an indicator of the blending behavior (Renzini 1998) and revealed that this problem is not important in most regions of the galaxy, as was indicated in Sect. 3.1, but it could be important for galactocentric distances lower than 2 Kpc. On the other hand, the bottom panel of Fig. 15 revealed a changing behavior of the stellar density. These results suggested that the trend observed in the upper panel could be mainly due to changes in the stellar density. However, in the central part of the galaxy, the blending effect and the high stellar densities would be a problem.

Regarding the stellar mass and bright distribution of the stellar groups, Bresolin et al. (1998) estimated an average V LF slope of 0.61 for the spiral galaxies mentioned at the beginning of this section. This value is considerably higher than our computation of 0.21. This discrepancy may be partly due to the different magnitude cutoff adopted in the slope measure ($M_V \leq -4.76$ in Bresolin et al. 1998, and $M_{F606W} \leq -3.81$ in our work). Additionally, the Bresolin et al. (1998) galaxies are much more distant than NGC 253 (between 6.7 and 14.5 Mpc), so it is probably that a blending effect is present affecting the objects magnitudes and consequently the LF shape. Studying only the most numerous groups with low errors in the fitted slope, that is those with more than 50 bright blue stars resulting from statistical decontamination and errors in the slopes lower than 0.09, we found that the

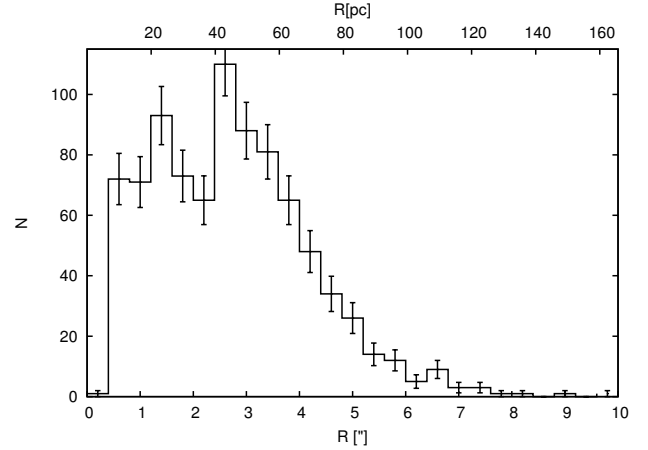


Figure 14. Size distribution of young star groups in NGC 253. Sizes in parsecs (upper edge) was computed adopted a distance of 3.56 Mpc (Tully et al. 2013).

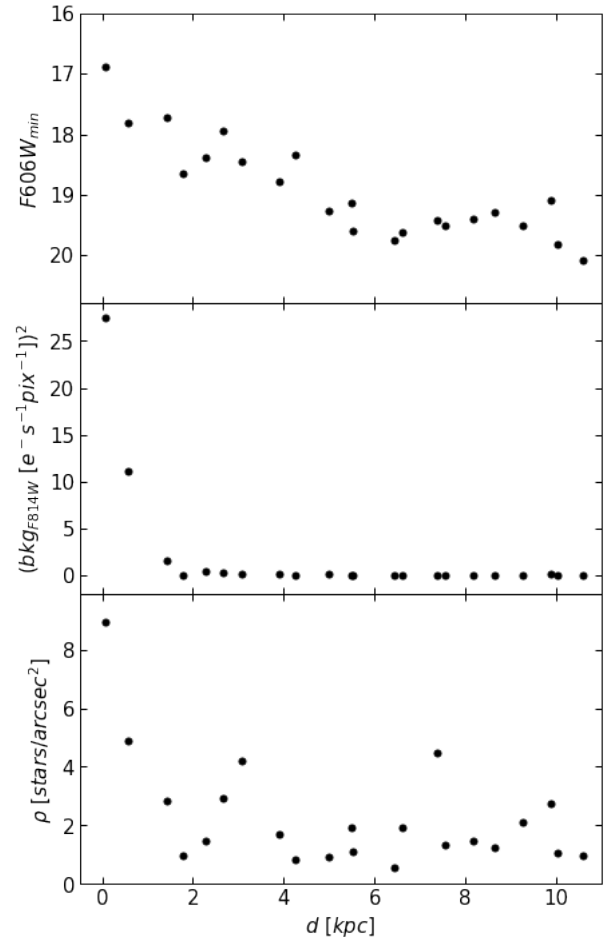


Figure 15. (Top panel:) Magnitude of the brightest star in the stellar groups, (Middle panel:) the red ($F814W$) background level and (Bottom panel:) the stellar density of stars brightest than $F606W = 24$, with respect to galactocentric distance. In the three panels was adopted a bin size of 0.5 kpc and were considered the same stellar groups.

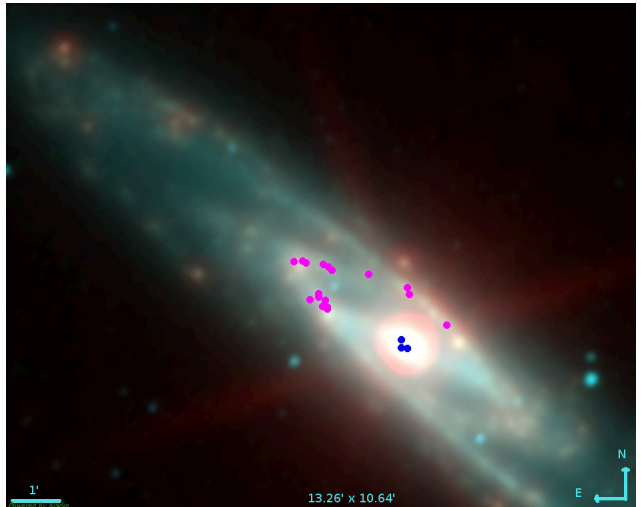
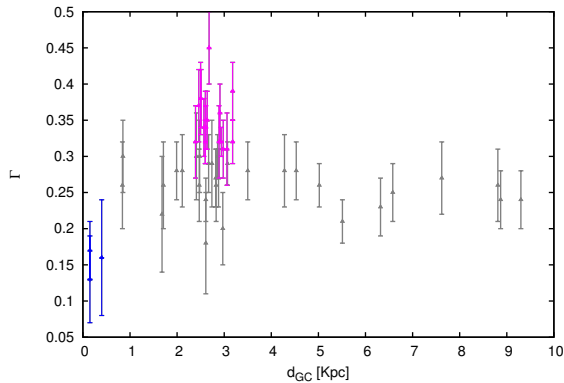


Figure 16. *Left:* Behavior of the LF slope with the galactocentric distance. Pink dots indicate groups with Γ values greater than 0.3. Blue points are groups with Γ values lower than 0.18. *Right:* Location of pink and blue dots over a Wise IR image of NGC 253. It can be clearly seen that the associations with low Γ values are found in the galactic core, while the ones with high values are located over an annular structure surrounding the galactic core.

groups with low slope values were located near the galactic center. On the other hand, groups with the highest slope values were located between ~ 2 -3.5 Kpc. The left panel of Fig. 16 shows the relationship of Γ and the galactocentric distance, in blue color were marked the groups with slope values lower than 0.18 and the slopes greater than 0.3 were marked in pink color. In the right panel of Fig. 16 we overlapped these associations on a IR WISE image of the galaxy. In this figure we can note that the groups with low values of the slope are near the galactic center, within the starburst region and inside complex A (see Fig. 12). These low values indicate that the LF slope is flatter than in the groups of other regions, so there would be more bright stars than in other groups, however this region is well correlated with the behavior presented in the middle panel of Fig. 15, therefore these values could be partially affected by the presence of blending. On the other hand, all the groups with slopes greater than 0.3 are over the annular structure that surrounds the bar and the nucleus, the LFs of these associations are characterized to have a large number of stars of weaker magnitudes.

Additionally, We estimated a mean density of 0.0006 stars/pc³ taking into account groups with more than 30 bright stars. It should be noted that this value was estimated counting stars with $M_{F606W} \leq -0.8$, which approximately correspond to the spectral type B6.

6 CONCLUSIONS

Using ACS/HST images we searched and identified young star groups in the starburst galaxy NGC 253. For this task, we first derived the absorption affecting different regions of the galaxy. After correcting by this effect, we used the PLC method over the blue bright objects to identify young groups and build the density map to detect larger young structures. A special designed code was run over the detected groups to estimate their fundamental parameters and to build their corresponding CMDs and LFs.

We constructed a catalog containing the characteristics of the 875 detected young groups. This catalog presents coordinates, sizes, number of members, densities, LF slopes and galactocentric distances.

Our study revealed that the groups detected are located over prominent structures of the galaxy, its nuclear region, the edge of the bar, a ring like structure that enclose the bar, and the spiral arms, confirming that all of them are star forming regions. The nuclear region of this galaxy had been greatly studied due to its starburst activity, it had been associated to a super star cluster by several authors. Nevertheless, we identified almost 20 different groups in this regions, suggesting that it is in fact a stellar complex. Additionally we found that this young population have a hierarchical behavior, in which the smaller groups are contained in larger structures.

The groups size distribution revealed a peak near 40 pc and an average radius of 47 pc, this values are consistent with those found in other galaxies. We also estimate a mean value of the $F606W$ LF slope of 0.21, with lower slope values in the galactic center and higher values in the ring structure, and an average density of 0.0006 stars/pc³ for stars considered earlier than B6.

ACKNOWLEDGEMENTS

We thank the referee for helpful comments and constructive suggestions that helped to improve this paper. MJR and GB acknowledge support from CONICET (PIP 112-201101-00301). MJR is a fellow of CONICET. This work was based on observations made with the NASA/ESA Hubble Space Telescope, and obtained from the Hubble Legacy Archive, which is a collaboration between the Space Telescope Science Institute (STScI/NASA), the Space Telescope European Coordinating Facility (ST-ECF/ESA) and the Canadian Astronomy Data Centre (CADN/NRC/CSA). Some of the data presented in this paper were obtained from the Mikulski Archive for Space Telescopes (MAST). STScI is

operated by the Association of Universities for Research in Astronomy, Inc., under NASA contract NAS5-26555. Support for MAST for non-HST data is provided by the NASA Office of Space Science via grant NNX09AF08G and by other grants and contracts. This publication makes use of data products from the Wide-field Infrared Survey Explorer, which is a joint project of the University of California, Los Angeles, and the Jet Propulsion Laboratory/California Institute of Technology, funded by the National Aeronautics and Space Administration. This research has made use of "Aladin sky atlas" developed at CDS, Strasbourg Observatory, France.

REFERENCES

- Battinelli P., 1991, *A&A*, 244, 69
- Bedin L. R., Piotto G., Baume G., Momany Y., Carraro G., Anderson J., Messineo M., Ortolani S., 2005, *A&A*, 444, 831
- Bianchi L., Efremova B., Hodge P., Kang Y., 2012, *AJ*, 144, 142
- Bresolin F., Kennicutt Jr. R. C., Stetson P. B., 1996, *AJ*, 112, 1009
- Bresolin F., et al., 1998, *AJ*, 116, 119
- Briceno C., 2008, *The Dispersed Young Population in Orion*. p. 838
- Chandar R., Bianchi L., Ford H. C., 1999, *ApJS*, 122, 431
- Dalcanton J., Williams B., ANGST Collaboration 2008, *The ACS Nearby Galaxy Survey Treasury: 9 Months of ANGST*. p. 115, doi:10.1007/978-1-4020-6933-8_24
- Davidge T. J., 2010, *ApJ*, 725, 1342
- Davidge T. J., 2016, *ApJ*, 818, 142
- Elmegreen B. G., Efremov Y., Pudritz R. E., Zinnecker H., 2000, *Protostars and Planets IV*, p. 179
- Engelbracht C. W., Rieke M. J., Rieke G. H., Kelly D. M., Achtermann J. M., 1998, *ApJ*, 505, 639
- Fernández-Ontiveros J. A., Prieto M. A., Acosta-Pulido J. A., 2009, *MNRAS*, 392, L16
- Fruchter A. S., Hook R. N., 2002, *PASP*, 114, 144
- Gaia Collaboration et al., 2016, *A&A*, 595, A2
- Gallart C., et al., 2003, *AJ*, 125, 742
- Garmany C. D., Stencel R. E., 1992, *A&AS*, 94, 211
- Gouliermis D., Kontizas M., Kontizas E., Korakitis R., 2003, *A&A*, 405, 111
- Hoopes C. G., Walterbos R. A. M., Greenwalt B. E., 1996, *AJ*, 112, 1429
- Iodice E., Arnaboldi M., Rejkuba M., Neeser M. J., Greggio L., Gonzalez O. A., Irwin M., Emerson J. P., 2014, *A&A*, 567, A86
- Kiss L. L., Bedding T. R., 2005, *MNRAS*, 358, 883
- Kornei K. A., McCrady N., 2009, *ApJ*, 697, 1180
- Massi F., Giannetti A., Di Carlo E., Brand J., Beltrán M. T., Marconi G., 2015, *A&A*, 573, A95
- Mel'Nik A. M., Efremov Y. N., 1995, *Astronomy Letters*, 21, 10
- Morau E., 2016, preprint, ([arXiv:1607.00027](https://arxiv.org/abs/1607.00027))
- Nantais J. B., Huchra J. P., McLeod B., Strader J., Brodie J. P., 2010, *AJ*, 139, 1413
- O'Donnell J. E., 1994, *ApJ*, 437, 262
- Ott J., Weiss A., Henkel C., Walter F., 2005, *ApJ*, 629, 767
- Pence W. D., 1980, *ApJ*, 239, 54
- Pietrzyński G., Gieren W., Fouqué P., Pont F., 2001, *A&A*, 371, 497
- Pietrzyński G., Ulaczyk K., Gieren W., Bresolin F., Kudritzki R. P., 2005, *A&A*, 440, 783
- Radovich M., Kahanpää J., Lemke D., 2001, *A&A*, 377, 73
- Renzini A., 1998, *AJ*, 115, 2459
- Rodríguez M. J., Baume G., Feinstein C., 2016, *A&A*, 594, A34
- Schlaflly E. F., Finkbeiner D. P., 2011, *ApJ*, 737, 103

Tang J., Bressan A., Rosenfield P., Slemer A., Marigo P., Girardi L., Bianchi L., 2014, *MNRAS*, 445, 4287

Tully R. B., et al., 2013, *AJ*, 146, 86

Vučetić M. M., Arbutina B., Urošević D., 2015, *MNRAS*, 446, 943

Watson A. M., et al., 1996, *AJ*, 112, 534

This paper has been typeset from a $\text{\TeX}/\text{\LaTeX}$ file prepared by the author.